



Cite this: *Analyst*, 2022, **147**, 2035

Received 31st March 2022,  
Accepted 29th April 2022

DOI: 10.1039/d2an00559j

rsc.li/analyst

## Single-particle spectroelectrochemistry: electrochemical tuning of plasmonic properties *via* mercury amalgamation in mesoporous silica coated gold nanorods without structural deformation†

Yola Yolanda Alizar<sup>a</sup> and Ji Won Ha  <sup>a,b</sup>

This paper elucidates the mercury (Hg) amalgamation induced by electrochemical reduction on gold nanorods coated with mesoporous silica shell (AuNRs@mSiO<sub>2</sub>) using single-particle spectroelectrochemistry. First, the silica shell significantly enhanced the structural stability of AuNR cores after Hg amalgamation with the application of linear sweep voltages (LSVs). Thus, we were able to focus on the spectral changes of AuNRs@mSiO<sub>2</sub> induced by the deposition of Hg without the disturbance of structural deformation, which also strongly affects localized surface plasmon resonance (LSPR) properties. Second, following the application of LSVs in the presence of Hg<sup>2+</sup>, a remarkable blueshift of the LSPR peak was observed, caused by the lowering of the work function due to the Hg adsorption, donating electron density to Au. Furthermore, the LSPR linewidth also dramatically increased after the Hg deposition with LSV. Lastly, the evolution of the Hg amalgamation process was directly observed by monitoring real-time LSPR peaks and LSPR linewidth shifts of a single AuNRs@mSiO<sub>2</sub> in the Hg solution according to the application of the electrochemical potential. Moreover, the results showed the possibility of the *in situ* tuning of the LSPR properties of AuNRs@mSiO<sub>2</sub> by Hg deposition *via* electrochemical potential manipulations without the disturbance of the structural variations of AuNR cores.

Mercury (Hg) is considered a toxic metal because it can easily accumulate in the body and damage organs such as the lungs, kidneys, liver, and brain even at small concentrations.<sup>1</sup> To date, extensive studies on reducing Hg concentrations in the environment have been conducted. Among these is the use of the amalgamation process, where plasmonic gold nano-

particles (AuNPs) are reacted with Hg with strong affinity. The formation of Au–Hg amalgams has been used for the accurate sensing of Hg with high toxicity<sup>2–7</sup> and water purification by removing Hg ions from polluted water.<sup>8–10</sup>

The direct observation of chemical reactions in AuNPs is of great importance to better understanding the processes for catalytic reaction and sensing applications.<sup>11</sup> So far, dark-field (DF) microscopy has been effectively used to directly observe and elucidate the reaction mechanisms of the chemical processes occurring on single AuNPs.<sup>11–13</sup> Recently, the DF setup was further combined with electrochemical cells to achieve the spectroscopic measurement of electrochemical processes on AuNP surfaces.<sup>11,14–17</sup> In this spectroelectrochemical approach, electrodes comprised of low-density AuNPs deposited on indium tin oxide (ITO) substrates were used to inject electrons into nanoparticles whose optical responses were then detected by DF microscopy and spectroscopy.<sup>11</sup> For example, the injected electrochemical charges enabled the modulation of the optical properties of anisotropic gold nanorods (AuNRs) at the single-particle level.<sup>14,15</sup>

Recently, several groups demonstrated the structural and spectral alterations according to the Hg deposition in the amalgamation process of bare AuNRs.<sup>11,13,18</sup> The AuNRs exposed to Hg were reshaped (from elongated to spherical nanoparticles) with the formation of Au–Hg amalgams, followed by a remarkable blueshift in the localized surface plasmon resonance (LSPR) peak. Thus, both the Hg deposition on the AuNRs and the shape deformation simultaneously affected the spectral variations. However, we recently presented Hg amalgamation *via* chemical reductions in AuNRs coated with mesoporous silica shell (AuNRs@mSiO<sub>2</sub>).<sup>19</sup> The mesoporous silica shell suppressed the structural deformation of the AuNR cores caused by the Au–Hg amalgamation. This enabled the monitoring of spectral responses according to the Hg deposition on the AuNR cores without the disturbance of shape deformations in single AuNRs@mSiO<sub>2</sub>. However, no studies have yet elucidated the structural and spectral

<sup>a</sup>Advanced Nano-Bio-Imaging and Spectroscopy Laboratory, Department of Chemistry, University of Ulsan, 93 Daehak-ro, Nam-gu, Ulsan 44610, Republic of Korea

<sup>b</sup>Energy Harvest-Storage Research Center (EHSRC), University of Ulsan, 93 Daehak-ro, Nam-gu, Ulsan, South Korea. E-mail: jwha77@ulsan.ac.kr; Fax: +82 52 712 8002; Tel: +82 52 712 8012

† Electronic supplementary information (ESI) available. See DOI: <https://doi.org/10.1039/d2an00559j>

variations of AuNRs@mSiO<sub>2</sub> induced by the electrochemical reduction of Hg in the amalgamation process with the application of the electrochemical potential.

The AuNRs@mSiO<sub>2</sub> used in this study were purchased from Nanopartz (CO, Loveland, USA). The morphologies of AuNRs@mSiO<sub>2</sub> were characterized using scanning electron microscopy (SEM). Fig. 1A shows a SEM image of AuNRs@mSiO<sub>2</sub>, and the size of the AuNR cores inside the mesoporous silica shell was determined to be 40(±2.4) nm × 121(±6.6) nm, as shown in Fig. 1B. An additional SEM image showing many AuNRs@mSiO<sub>2</sub> is provided in Fig. S1.† Moreover, the thickness of the mesoporous silica shell was about 22 nm (Fig. S2†). Fig. 1C shows an ultraviolet-visible (UV-Vis) extinction spectrum of AuNRs@mSiO<sub>2</sub> in distilled water, and two transverse and longitudinal LSPR peaks of the AuNR cores are seen at approximately 530 and 723 nm, respectively.

In this study, we employed a single-particle spectroelectrochemistry approach to investigate the Hg amalgamation in single AuNRs@mSiO<sub>2</sub> deposited on an ITO glass. Spectroelectrochemistry is a powerful technique based on DF microscopy and spectroscopy coupled to an electrochemical workstation.<sup>11,15–17</sup> DF microscopy and spectroscopy are used to detect changes in the optical properties of single nanoparticles, whereas the electrochemical potential is applied to nanoparticles on an ITO glass. An experimental setup for DF microscopy-based spectroelectrochemistry is shown in Fig. 2A. A spectroelectrochemical cell (SEC, Fig. 2B) was built with the ITO coverslip as the working electrode (WE), platinum (Pt) wire with 0.076 mm diameter as the counter electrode (CE), and an

**A** **Spectroelectrochemistry:**  
DF Microscopy with Electrochemistry

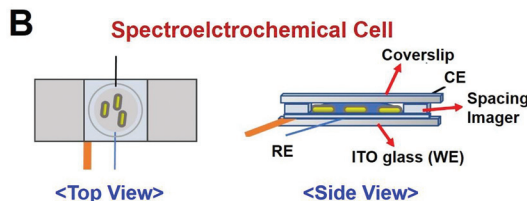
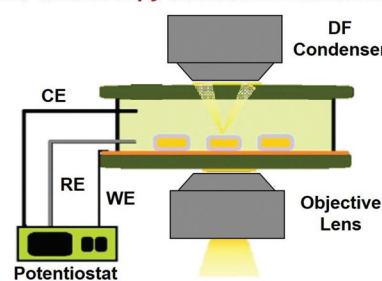


Fig. 2 (A) A schematic showing the experimental setup of the DF microscopy coupled with an electrochemical workstation. (B) Spectroelectrochemical cell diagram with ITO-coated glass as the working electrode (WE), Pt wire CE, insulated Pt quasi-reference electrode (RE), and spacing imager.

insulated Pt wire (AM Systems) as the quasi-reference electrode (RE).

In this study, AuNRs@mSiO<sub>2</sub> were deposited on an ITO WE that can inject electrons to nanoparticles through electrochemical potential manipulation (Fig. 3A). Thus, this study used the reduction of Hg<sup>2+</sup> through electrochemical injection in the absence of any chemical reductant (e.g., NaBH<sub>4</sub>), and the direct Hg amalgamation of AuNRs@mSiO<sub>2</sub> was studied through a spectroelectrochemistry approach (Fig. 3A).

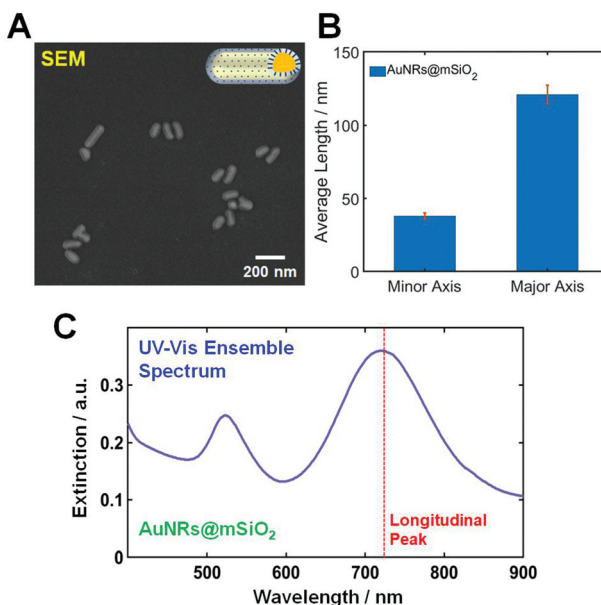
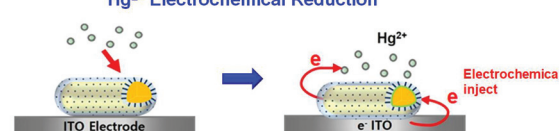


Fig. 1 (A) SEM image of AuNRs@mSiO<sub>2</sub>. (B) Histogram showing the size distribution of AuNRs@mSiO<sub>2</sub>. (C) UV-Vis extinction spectrum of AuNRs@mSiO<sub>2</sub>. The red-dotted line indicates the position of the longitudinal LSPR peak.

**A** **Hg<sup>2+</sup> Electrochemical Reduction**



**B** **SEM Image After LSV**

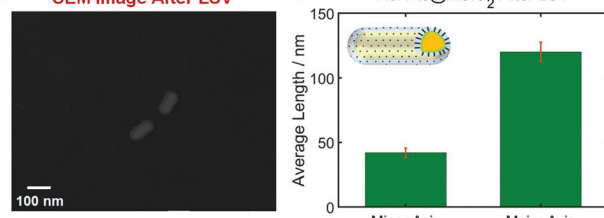


Fig. 3 (A) Schematic depiction of Hg<sup>2+</sup> electrochemical reduction occurring on the AuNR core inside the mesoporous silica shell on an ITO glass. (B) SEM image of AuNRs@mSiO<sub>2</sub> after LSV in the presence of 10  $\mu$ M HgCl<sub>2</sub>. (C) Histogram showing the change in the sizes (length and width) of AuNRs@mSiO<sub>2</sub> after LSV and Hg amalgamation.

Recently, morphological changes were reported according to the Hg amalgamation of anisotropic AuNRs.<sup>13,18</sup> Bare AuNRs exposed to Hg were reshaped from elongated nanoparticles to spherical nanoparticles, which can affect their LSPR properties. Furthermore, we recently reported that the mesoporous silica shell in AuNRs@mSiO<sub>2</sub> enhanced the structural stability of the AuNR cores against shape deformation induced by Hg amalgamation.<sup>19</sup> However, no studies have yet reported the structural stability of AuNRs@mSiO<sub>2</sub> according to electrochemical Hg amalgamation with the application of the electrochemical potential to nanoparticles.

We first checked the structural variations of the AuNRs@mSiO<sub>2</sub> after applying LSVs in the presence of HgCl<sub>2</sub>. SEM images of AuNRs@mSiO<sub>2</sub> were obtained 1 h after their exposure to a Hg solution with LSVs. As shown in Fig. 3B and S3†, the aspect ratio (AR) of the AuNRs@mSiO<sub>2</sub> was not decreased after the Hg amalgamation with LSVs. This result is clearly different from that of bare AuNRs, which display major structural deformations after amalgamation.<sup>11,13,18</sup> Before the Hg amalgamation, the average AR of the AuNRs@mSiO<sub>2</sub> was 3.02(±1.21), corresponding to 40(±2.4) nm in width and 121(±6.6) nm in length, respectively (Fig. 1B). After the electrochemical Hg amalgamation in the presence of 0.1 M potassium chloride (KCl) as the supporting electrolyte and 10 μM HgCl<sub>2</sub> for 1 h, the average AR was approximately 2.93, corresponding to 41(±3.5) nm in width and 120(±7.5) nm in length, respectively (Fig. 3C). Therefore, we confirmed that the silica shell significantly enhanced the structural stability of AuNRs despite the electrochemical Hg amalgamation, which induces significant structural deformation. This result is consistent with our recent study on chemical reduction in the Hg amalgamation of AuNRs@mSiO<sub>2</sub>.<sup>19</sup>

Next, we investigated the LSPR spectral changes of AuNRs@mSiO<sub>2</sub> before and after Hg amalgamation *via* electrochemical reduction under the DF microscopy combined with an electrochemical workstation (Fig. 2 and S4†). DF images were obtained before and after the application of cathodic linear potential sweeps, and they were correlated with the overall current profiles acquired in the applied potential range of 0.3 to −0.7 V (vs. Pt). Fig. 4A shows a DF scattering image of single AuNRs@mSiO<sub>2</sub> on the ITO glass before applying LSV in absence of Hg<sup>2+</sup>. Afterward, SECs with AuNRs@mSiO<sub>2</sub> on the ITO were filled with 0.1 M KCl as the supporting electrolyte and 10 μM HgCl<sub>2</sub>. With the application of LSV in the presence of 0.1 M KCl and 10 μM HgCl<sub>2</sub>, Hg<sup>2+</sup> was electrochemically reduced, and Hg atoms were deposited on the AuNR surfaces to form AuNRs@Hg-mSiO<sub>2</sub> (core@shell) (Fig. 4B). A major advantage of using AuNRs@mSiO<sub>2</sub> in this study is that we can directly reveal their LSPR spectral changes by focusing on the effect of Hg deposition without considering the effects of structural variations driven by Hg deposition that can also strongly affect the LSPR properties.

We first obtained linear sweep voltammograms to confirm the electrochemical reduction of Hg<sup>2+</sup>, as shown in Fig. 4C. The electrochemical potential varied from 0.3 to −0.7 V (vs. Pt) during LSV. The current–voltage profile acquired without Hg<sup>2+</sup>

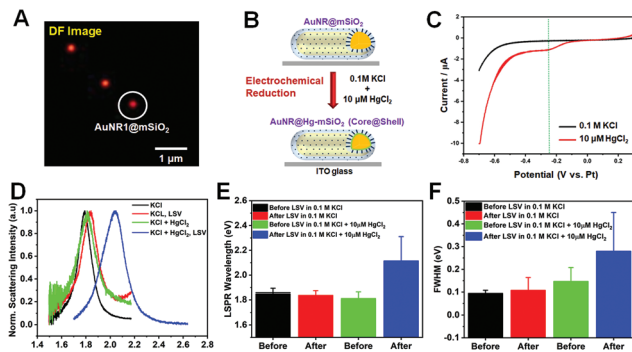


Fig. 4 (A) DF scattering image of AuNRs@mSiO<sub>2</sub>. (B) A schematic depicting the electrochemical reduction on a AuNR@mSiO<sub>2</sub> in the presence of 0.1 M KCl and 10 μM HgCl<sub>2</sub>. (C) Linear sweep voltammograms obtained in 0.1 M KCl (black curve) and in the solution of 0.1 M KCl and 10 μM HgCl<sub>2</sub> (red curve). (D) Scattering spectra of AuNR1@mSiO<sub>2</sub> before and after LSV in 0.1 M KCl and in 0.1 M KCl and 10 μM HgCl<sub>2</sub>. (E) Histogram showing the change in LSPR wavelength of AuNRs@mSiO<sub>2</sub> before and after LSV in 0.1 M KCl and in 0.1 M KCl and 10 μM HgCl<sub>2</sub>. (F) Histogram showing the change in the LSPR linewidth (FWHM) of AuNRs@mSiO<sub>2</sub> before and after LSV in 0.1 M KCl and in 0.1 M KCl and 10 μM HgCl<sub>2</sub>. The reference electrode was a Pt wire.

is shown in the black curve, indicating the absence of faradaic currents. The red curve was recorded after the introduction of 10 μM Hg<sup>2+</sup>. A peak was observed at approximately −0.25 V (green dotted line in Fig. 4C), attributed to the electrochemical reduction of Hg<sup>2+</sup> to Hg<sup>0</sup>. We further confirmed that the reduction peak weakened when the concentration of Hg<sup>2+</sup> was decreased to 5 μM, as demonstrated in Fig. S5A and B.† Therefore, we ensured that the electrochemical reduction occurred in SEC with the application of LSV in this study.

DF scattering spectra were then recorded for single AuNRs@mSiO<sub>2</sub> before and after the application of the electrochemical potential. Fig. 4D shows the single-particle scattering spectra of a AuNR1@mSiO<sub>2</sub> indicated by a white circle in Fig. 4A. The initial LSPR spectrum of the circled AuNR1@mSiO<sub>2</sub>, characterized by an LSPR wavelength of 1.75 eV and an FWHM of 109 meV, exhibited no drastic optical variations after LSV in the pure electrolyte (red curve) and after the introduction of Hg<sup>2+</sup> to the SEC (green curve). However, following the application of LSV in the presence of Hg<sup>2+</sup>, dramatic variations were observed in the scattering spectrum (blue curve). As shown in Fig. 4D, after the Hg amalgamation with LSV, the LSPR wavelength blueshifted from 1.75 to 2.13 eV. This result is further supported by the ensemble spectra of AuNRs@mSiO<sub>2</sub> obtained before and after Hg amalgamation (Fig. 1C and S5†). Because AuNRs@mSiO<sub>2</sub> are stable against the structural deformation induced by the Hg amalgamation (Fig. 3), the blueshift shown for AuNRs@mSiO<sub>2</sub> after Hg amalgamation can be attributed mainly to the lowering of the work function due to the Hg adsorption, donating electron density to Au.<sup>20</sup> Furthermore, the LSPR linewidth (or FWHM) can also provide important information on plasmon damping in single AuNRs.<sup>21–25</sup> The LSPR linewidth of AuNR1@mSiO<sub>2</sub> showed a

dramatic increase to 246 meV after the Hg deposition with LSV (Fig. 4D). The strong plasmon damping observed for single AuNRs@mSiO<sub>2</sub> in this study was caused by the Hg deposition on the AuNR surface.<sup>19</sup>

Additionally, we measured 30 more single AuNRs@mSiO<sub>2</sub> under the same experimental conditions to verify the tendency shown in Fig. 4D. We observed significant optical changes after applying LSV in the presence of Hg<sup>2+</sup> (blue bar, Fig. 4E), consistent with the result for AuNR1@mSiO<sub>2</sub> in Fig. 4D. A dramatic blueshift of the LSPR wavelength from 1.798 eV (green bar) to 2.167 eV (blue bar) was observed when LSV was applied in the presence of 10 μM Hg<sup>2+</sup> caused, as shown in Fig. 4E. Similarly, the same result (or tendency) was obtained for AuNRs@mSiO<sub>2</sub> in a small concentration of 5 μM Hg<sup>2+</sup> (Fig. S6†). We also confirmed that, in addition to the LSPR wavelength, the FWHM was remarkably increased after the Hg deposition on the AuNR cores *via* the application of LSV in AuNRs@mSiO<sub>2</sub>. The LSV application in the presence of 10 μM Hg<sup>2+</sup> remarkably broadened the LSPR linewidth from 145 meV (green bar) to 279 meV (blue bar), as shown in Fig. 4E. Therefore, the results provide deeper insight into the effect of Hg deposition by electrochemical reduction on spectral changes in single AuNRs@mSiO<sub>2</sub> without structural deformation and disturbance.

Single-particle spectroscopy enables gaining insight into the time-dependent adsorption kinetics of Hg ions on AuNR cores. Thus, the evolution of the Hg amalgamation process was directly observed by acquiring the real-time scattering spectra of single AuNRs@mSiO<sub>2</sub> in the presence of 10 μM Hg<sup>2+</sup> to better understand LSPR spectral changes caused by Hg amalgamation. Initially, the applied potential was kept constant, and then linear cathodic potential sweeps and open-cell voltage (OCV) conditions were applied. Representative potential *vs.* time and current *vs.* time curves subjected to electrochemical measurements (linear sweep voltammetry) are shown for a single AuNR@mSiO<sub>2</sub> in the solution of 0.1 M KCl and 10 μM HgCl<sub>2</sub> (Fig. 5A). In addition, the curves are correlated with a two-dimensional (2D) plot obtained from 500 scattering spectra acquired *in situ* for 500 s (1 spectrum per s). In the real-time analysis of the Hg amalgamation process, the LSPR wavelength remained constant during the first 190 s when the potential of 0.2 V (*vs.* Pt) was applied constantly. Afterwards, a slight increase of the LSPR wavelength was observed between 190 s and 200 s when the applied potential was remained constant at 0.3 V (*vs.* Pt). Finally, the LSPR wavelength slightly blueshifted between 200 and 300 s when the linear potential scan was applied from 0.3 to −0.7 V (*vs.* Pt, LSV), followed by the use of the OCV condition. In addition, the FWHM increased concomitantly with the recorded blueshift arising from the application of a cathodic potential scan. LSPR peak changes before, during, and after LSV are clearly observed in single-particle scattering spectra of the nanoparticle (Fig. 5B). The LSPR peak slightly blueshifted with the LSPR linewidth broadening during the application of LSV (Fig. 5C). The spectral changes are related to the deposition of Hg on the AuNR surface with the formation of a core–shell structure. Therefore, we monitored the *in situ* time-dependent spectral changes

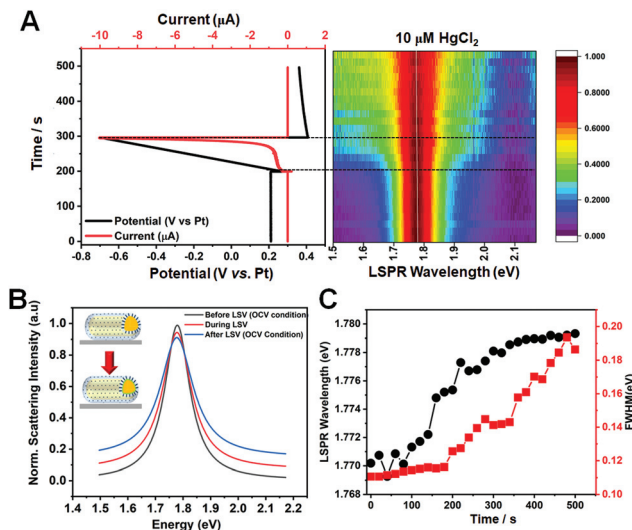


Fig. 5 (A) Potential *vs.* time and current *vs.* time curves correlated with a 2D plot of 500 scattering spectra recorded *in situ* at a single AuNR@mSiO<sub>2</sub> in 0.1 M KCl and 10 μM HgCl<sub>2</sub>. The applied potential was initially held at 0.2 V (*vs.* Pt) and then 0.3 V (*vs.* Pt), followed by the application of linear cathodic potential sweeps from 0.3 to −0.7 V (*vs.* Pt) and, finally, open-cell voltage conditions. (B) Scattering spectra of a AuNR@mSiO<sub>2</sub> before (black curve), during (red curve), and after (blue curve) LSV. (C) LSPR wavelength and FWHM shifts as functions of time during the application of potential energy.

(LSPR wavelength and FWHM) caused by the formation of Hg-coated core–shell AuNRs (AuNRs@Hg–mSiO<sub>2</sub>) through single-particle measurements.

Two important points must be further discussed in Fig. 5. First, Schopf *et al.* reported morphological and spectral changes according to the Hg concentration in the amalgamation of bare AuNRs.<sup>11,13</sup> AuNRs exposed to Hg were reshaped to spherical nanoparticles with the formation of Au–Hg amalgams, accompanied by a remarkable blueshift in the LSPR peak. In contrast, the AuNRs@mSiO<sub>2</sub> used in this study were stable against structural deformations caused by the Hg amalgamation and LSV because of the silica shell. Therefore, we investigated the spectral changes of AuNRs@mSiO<sub>2</sub> induced by the deposition of Hg without the disturbance of morphological variation, which also strongly affects the LSPR properties. Second, so far, various attempts have been made to tune the LSPR properties of metal nanostructures using the electrochemical method.<sup>26–30</sup> A feature of the electrochemical potential control method is its ability to change the absolute potential of the electrons in metal nanostructures, which can cause a resonance energy shift. For instance, Oikawa *et al.* reported the control of electrochemical copper deposition or dissolution reactions at the surface of Au nanostructures.<sup>27,30</sup> Similarly, the present study showed the possibility of *in situ* tuning of the LSPR properties (resonance energy and LSPR linewidth) of AuNRs@mSiO<sub>2</sub> through Hg deposition *via* electrochemical potential manipulation without the disturbance of spectral variation caused by Hg-induced structural deformations (Fig. 5).

In summary, we investigated the Hg amalgamation induced by electrochemical reduction on AuNRs@mSiO<sub>2</sub> using single-particle spectroelectrochemistry. First, the silica shell significantly enhanced the structural stability of the AuNR cores after LSV for the Hg amalgamation. Thus, we were able to focus on the spectral changes of AuNRs@mSiO<sub>2</sub> induced by the deposition of Hg without the disturbance of structural changes, which can also strongly affect the LSPR properties. Second, following the application of LSV in the presence of Hg<sup>2+</sup>, dramatic changes occurred in the scattering spectrum. After the Hg amalgamation with LSV, a dramatic blueshift of LSPR peak was observed, caused by the lowering of the work function due to the Hg adsorption, donating electron density to Au. Furthermore, the LSPR linewidth also dramatically increased after the Hg deposition with LSV. Lastly, we directly observed the evolution of the Hg amalgamation process by monitoring real-time LSPR peaks and FWHM shifts of single AuNRs@mSiO<sub>2</sub> in the Hg solution during LSV. In addition, the present study showed the possibility of the *in situ* tuning of LSPR spectral properties (characteristic resonance energy and LSPR linewidth) of AuNRs@mSiO<sub>2</sub> through Hg deposition *via* electrochemical potential manipulation without the disturbance of spectral variations caused by Hg-induced structural deformations.

## Author contributions

Y. Y. Alizar performed all the experiments. Y. Y. Alizar and J. W. Ha analyzed the data. Y. Y. Alizar and J. W. Ha wrote the manuscript.

## Conflicts of interest

There are no conflicts to declare.

## Acknowledgements

This work was supported by two National Research Foundation of Korea (NRF) grants funded by the Korean government (MSIP) (No. 2018R1C1B3001154 and No. 2019R1A6A1A11053838).

## Notes and references

- 1 C. T. Driscoll, R. P. Mason, H. M. Chan, D. J. Jacob and N. Pirrone, *Environ. Sci. Technol.*, 2013, **47**, 4967–4983.
- 2 M. Rex, F. E. Hernandez and A. D. Campiglia, *Anal. Chem.*, 2006, **78**, 445–451.
- 3 H. Huang, C. Qu, X. Liu, S. Huang, Z. Xu, Y. Zhu and P. K. Chu, *Chem. Commun.*, 2011, **47**, 6897–6899.
- 4 A. Singh, R. Pasricha and M. Sastry, *Analyst*, 2012, **137**, 3083–3090.
- 5 J. Z. James, D. Lucas and C. P. Koshland, *Environ. Sci. Technol.*, 2012, **46**, 9557–9562.
- 6 L. Deng, X. Ouyang, J. Jin, C. Ma, Y. Jiang, J. Zheng, J. Li, Y. Li, W. Tan and R. Yang, *Anal. Chem.*, 2013, **85**, 8594–8600.
- 7 J. R. Crockett, H. Win-Piazza, J. E. Doebler, T. Luan and Y. Bao, *ACS Appl. Nano Mater.*, 2021, **4**, 1654–1663.
- 8 I. Ojea-Jiménez, X. López, J. Arbiol and V. Puntes, *ACS Nano*, 2012, **6**, 2253–2260.
- 9 S.-I. Lo, P.-C. Chen, C.-C. Huang and H.-T. Chang, *Environ. Sci. Technol.*, 2012, **46**, 2724–2730.
- 10 S. Pacheco, M. Medina, F. Valencia and J. Tapia, *J. Environ. Eng.*, 2006, **132**, 342–349.
- 11 C. Schopf, A. Wahl, A. Martín, A. O'Riordan and D. Iacopino, *J. Phys. Chem. C*, 2016, **120**, 19295–19301.
- 12 C. Novo, A. M. Funston and P. Mulvaney, *Nat. Nanotechnol.*, 2008, **3**, 598–602.
- 13 C. Schopf, A. Martín, M. Schmidt and D. Iacopino, *J. Mater. Chem. C*, 2015, **3**, 8865–8872.
- 14 C. Novo, A. M. Funston, A. K. Gooding and P. Mulvaney, *J. Am. Chem. Soc.*, 2009, **131**, 14664–14666.
- 15 B. S. Hoener, H. Zhang, T. S. Heiderscheit, S. R. Kirchner, A. S. De Silva Indrasekara, R. Baiyasi, Y. Cai, P. Nordlander, S. Link, C. F. Landes and W.-S. Chang, *J. Phys. Chem. Lett.*, 2017, **8**, 2681–2688.
- 16 B. S. Hoener, C. P. Byers, T. S. Heiderscheit, A. S. De Silva Indrasekara, A. Hoggard, W.-S. Chang, S. Link and C. F. Landes, *J. Phys. Chem. C*, 2016, **120**, 20604–20612.
- 17 J.-G. Wang, J. S. Fossey, M. Li, T. Xie and Y.-T. Long, *ACS Appl. Mater. Interfaces*, 2016, **8**, 8305–8314.
- 18 J. Lee, G. W. Kim and J. W. Ha, *Analyst*, 2022, **147**, 1066–1070.
- 19 G. W. Kim and J. W. Ha, *J. Phys. Chem. Lett.*, 2022, **13**, 2607–2613.
- 20 T. Morris, K. Kloepper, S. Wilson and G. Szulczewski, *J. Colloid Interface Sci.*, 2002, **254**, 49–55.
- 21 H. B. Jeon, S. Park, K. R. Ryu, S. K. Ghosh, J. Jung, K. M. Park and J. W. Ha, *Chem. Sci.*, 2021, **12**, 7115–7124.
- 22 S. Y. Lee, P. V. Tsai, G. W. Kim, M. J. Seo, J. W. Hong and J. W. Ha, *Nano Lett.*, 2019, **19**, 2568–2574.
- 23 S. W. Moon, P. V. Tsai and J. W. Ha, *Phys. Chem. Chem. Phys.*, 2018, **20**, 22197–22202.
- 24 K. R. Ryu, D. H. Nam, S. Lee and J. W. Ha, *J. Phys. Chem. C*, 2020, **124**, 14818–14825.
- 25 C. Novo, D. Gomez, J. Perez-Juste, Z. Zhang, H. Petrova, M. Reismann, P. Mulvaney and G. V. Hartland, *Phys. Chem. Chem. Phys.*, 2006, **8**, 3540–3546.
- 26 A. M. Brown, M. T. Sheldon and H. A. Atwater, *ACS Photonics*, 2015, **2**, 459–464.
- 27 S. Oikawa, H. Minamimoto, X. Li and K. Murakoshi, *Nanotechnology*, 2017, **29**, 045702.
- 28 H. Minamimoto, S. Oikawa, T. Hayashi, A. Shibasaki, X. Li and K. Murakoshi, *J. Phys. Chem. C*, 2018, **122**, 14162–14167.
- 29 A. Henkel, A. Jakab, G. Brunklaus and C. Sönnichsen, *J. Phys. Chem. C*, 2009, **113**, 2200–2204.
- 30 S. Oikawa, H. Minamimoto and K. Murakoshi, *Chem. Lett.*, 2017, **46**, 1148–1150.